PLINDER:
The protein-ligand interactions dataset and evaluation resource

Janani Durairaj [* 1 2] **Yusuf Adeshina** [* 3] **Zhonglin Cao** [4] **Xuejin Zhang** [3] **Vladas Oleinikovas** [3]
Thomas Duignan [3] **Zachary McClure** [4] **Xavier Robin** [1 2] **Emanuele Rossi** [3] **Guoqing Zhou** [4] **Srimukh Veccham** [4]
Clemens Isert [3] **Yuxing Peng** [4] **Prabindh Sundareson** [4] **Mehmet Akdel** [3] **Gabriele Corso** [5] **Hannes Stärk** [5]
Zachary Carpenter [3] **Michael Bronstein** [3 6] **Emine Kucukbenli** [4] **Torsten Schwede** [1 2] **Luca Naef** [3]

Abstract

Protein-ligand interactions (PLI) are foundational to small molecule drug design. With computational methods striving towards experimental accuracy, there is a critical demand for a well-curated and diverse PLI dataset. Existing datasets are often limited in size and diversity, and commonly used evaluation sets suffer from training information leakage, hindering the realistic assessment of method generalization capabilities. To address these shortcomings, we present PLINDER, the largest and most annotated dataset to date, comprising 449,383 PLI systems, each with over 500 annotations, similarity metrics at protein, pocket, interaction and ligand levels, and paired unbound (*apo*) and predicted structures. We propose an approach to generate training and evaluation splits that minimizes task-specific leakage and maximizes test set quality, and compare the resulting performance of DiffDock when retrained with different kinds of splits.

1. Introduction

The protein-ligand field has seen a surge in the application of deep learning-based prediction methods, notably in tasks such as **rigid body docking** (Stärk et al., 2022; Lu et al., 2022; Corso et al., 2023) where the pose of a ligand within a given rigid protein structure is predicted, **flexible pocket docking** (Plainer et al., 2023; Qiao et al., 2024) which allows side-chain movements of pocket residues, **co-folding** (Qiao et al., 2024; Krishna et al., 2024; Abramson et al.,

2024) where both the protein conformation and ligand pose are predicted at once, **pocket-conditioned ligand generation** (Schneuing et al., 2023) where novel ligand molecules are generated within a given protein structure and pocket, **ligand-conditioned protein engineering** (Dauparas et al., 2023) where, conversely, novel protein sequences are designed to selectively bind a ligand, and **molecular scaffolding** (Chawdhury et al., 2021) where ligands are modified to enhance their affinity to a protein or pocket.

These methods hold promise in accelerating drug discovery and protein engineering by facilitating the accurate prediction of ligand binding poses within protein structures. However, their effectiveness relies heavily on the datasets used for training and evaluation, where several key considerations must be addressed: **1. Training set diversity** to move to high data regimes and learn the underlying patterns instead of simple memorization; **2. Low information leakage between train and test** to accurately assess generalisation capabilities and avoid inflating expected performance by over-fitting; **3. Test set quality** to avoid comparing prediction results to unreliable ground truth caused by varying experimental quality or missing atoms in and around the binding site; **4. Test set diversity** to showcase performance across a range of complex types and use-cases; and **5. Realistic inference scenarios** to move beyond the "re-docking" use-case where the ligand pose is predicted within the never-available experimental ligand-bound receptor conformation.

Despite the availability of numerous publicly reported protein-ligand interaction (PLI) structural datasets, many fall short in meeting these critical considerations. For instance, BioLip2 (Zhang et al., 2024), a sizable dataset, primarily emphasizes functional annotation and lacks suitable partitioning for training or testing machine learning-based methods. Other datasets such as PDBBind (Wang et al., 2005) and variants of it come with suggested splits, yet they are small and contains information leakage between data partitions. Attempts to address leakage issues in PDBBind remain limited in dataset size and do not provide principled evaluation of different leakage metrics chosen via model

---

[*]Equal contribution [1]Biozentrum, University of Basel, Basel, Switzerland [2]SIB: Swiss Institute of Bioinformatics, Basel, Switzerland [3]VantAI, New York, USA [4]NVIDIA [5]MIT CSAIL [6]Oxford University. Correspondence to: Janani Durairaj <janani.durairaj@unibas.ch>, Yusuf Adeshina <yusuf@vant.ai>.

retraining (Li et al., 2024). Selectively combining previously curated datasets using evolutionary classification of protein domains (ECOD) (Cheng et al., 2014) annotations, as done in DockGen (Corso et al., 2024), ensures novel test domains to assess generalization potential, but is still limited in dataset size, constrained by manual curation biases in ECOD domain annotation, and has limitations in assessing novel ligands and binding modes for shared ECOD domains.

PLINDER offers the largest and most diverse dataset of protein-ligand complexes, encompassing various types such as multi-ligand systems, oligonucleotides, peptides, and saccharides. It calculates similarity between complexes at the protein, pocket, PLI, and ligand levels, enabling the measurement of diversity and detection of information leakage. Additionally, PLINDER annotates complexes for quality and domain information, and proposes an approach to prioritize a diverse, high-quality test set with minimal leakage. It also links *holo* complexes to relevant *apo* and predicted structures, facilitating realistic inference scenarios. Through these measures, PLINDER aims to provide researchers in the protein-ligand field with a robust and reliable dataset for training and evaluating deep learning-based prediction methods, ultimately advancing the development of novel drug discovery and protein engineering approaches.

2. Method Overview

2.1. Dataset Curation and Annotation

We obtained all entries from the Protein Data Bank (PDB) (Berman et al., 2000) as of 2024-04-09, using MMCIF files in the PDB NextGen Archive resource (Choudhary et al., 2023). For entries solved by X-ray crystallography, we extracted entry and residue-level information from the corresponding X-ray validation reports. We generated each biounit assembly of each PDB entry using OpenStructure (Biasini et al., 2013), and obtained all protein-ligand interactions detected by the protein-ligand interaction profiler (PLIP) (Adasme et al., 2021) for all ligand-like chains. Only interactions between protein and ligand atoms or ligand atoms and water molecules are considered. A chain within a PDB entry was labelled as a ligand chain if one of the following was true: (1) the chain type was non-polymer, (2) there was a Biologically Interesting Molecule Reference Dictionary (BIRD) (Dutta et al., 2014) identifier associated with that chain, (3) the chain was of type polypeptide, oligosaccharide, or oligonucleotide and had less than 10 residues, (4) the chain was of type polypeptide and had less than 20 residues and no UniProt ID associated with it. Ligand chains within 4 Å of each other or having a detectable PLIP interaction are merged into the same PLI system. Each system is also associated with its "interacting" residues, consisting of residues participating in a PLIP interaction with the ligand chains of that system, and "neighboring" residues, consisting of residues within 6 Å of the ligand, together making up the system pocket. Thus, PLI systems are defined by the combination of a PDB ID, biounit identifier, specific instance(s) of the ligand chain(s), and specific instance(s) of the interacting protein chain(s) (Figure 1A).

For each system, we provide annotations broadly categorised in Table A. All domain annotations are mapped to pocket residues, and the domain sharing the highest overlap with the pocket is retained as the pocket domain. Systems are labelled as *holo*, artifact or ion and annotated with ligand definitions and properties as described in Appendix A.1. We performed extensive molecule processing and cleaning efforts to correct bond, valence and chirality issues to ensure that the vast majority of PLINDER can readily be processed and used by the typical pre-processing and feature extraction routines employed by deep learning methods, and those which cannot are clearly annotated.

2.2. Protein-ligand system similarity

To cluster and split our curated dataset, we calculated protein and pocket similarity using MMSeqs (Steinegger & Söding, 2017) and Foldseek (van Kempen et al., 2024) (Figure 1B), PLI similarity using the alignments combined with unique PLIP interactions, and ligand similarity using ECFP4 fingerprints. MMSeqs and Foldseek searches were conducted on all PDB chains within all systems (E-value < 0.01, min_seq_id 0.2, max_seqs 5000) to yield alignments and query coverages. Protein similarities are determined based on lDDT score (only for Foldseek), identity percentage, sequence similarity, and query coverage-adjusted global versions of these scores. Per-residue alignment information was used to calculate pocket-level scores. PLIP interactions were made unique using the interaction type and type-specific attributes as defined in Table A9, and combined with pocket information in a weighted Jaccard similarity metric to compute a PLI-level similarity measure. See Appendix B for more details.

For each similarity metric and given thresholds (50, 70, 95, 100), a graph is created with systems as nodes and edges between systems which have a similarity score above the threshold for the specified metric. Note that all similarity values are adapted to be in the 0-100 range. Strong and weakly connected components, as well as communities based on the Parallel Louvain Method are identified for this graph, using NetworKit (Angriman et al., 2023), and systems within each cluster are labelled with the corresponding cluster identifier, adding additional similarity-centric annotations to each system.

2.3. Train-validation-test dataset splitting

We used Algorithm 1 to split the dataset into proto-train and test sets, to ensure that our requirements for training set
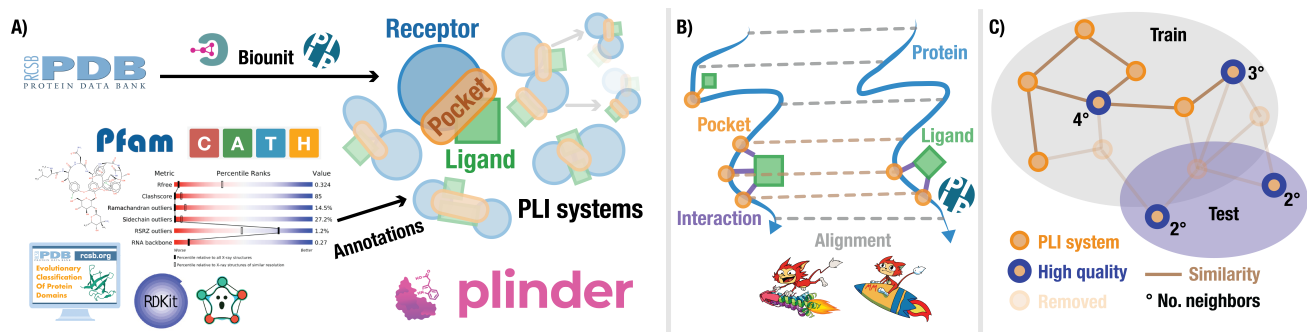
Figure 1. **A)** Curation and annotation of PLI systems from the PDB, **B)** Measuring similarity between PLI systems **C)** Splitting into diverse train and high quality test sets.

Algorithm 1 Splitting

1: **Input:** systems S, clusters C, graphs G, depths D, maximum leakage count M, minimum cluster size m, number of representatives from each cluster n
2: **Output:** $proto\_train$ and $test$ systems
3: Initialize $proto\_test \leftarrow \emptyset$
4: Initialize $\forall s \in S, N_s = \emptyset$
5: **for** $s \in S$ **do**
6:     **if** $pass\_quality(s)$ **then**
7:         **for** $g = 1$ to $|G|$ **do**
8:             $N_s \leftarrow N_s \bigcup neighbors\_upto\_depth(s, G_g, D_g)$
9:         **if** $m < |N_s| < M$ **then**
10:            $proto\_test.insert(s)$
11: Sort $s \in proto\_test$ by $|N_s|$
12: Initialize $test \leftarrow \emptyset$
13: **for** $c \in C$ **do**
14:     $test \leftarrow$ up to n from $proto\_test$ for c
15: Initialize $proto\_train \leftarrow S$
16: **for** $s \in test$ **do**
17:     $proto\_train \leftarrow proto\_train \setminus N_s$

---

size, test set quality, test set diversity, and low information leakage are met (Figure 1C). It is important to note that these considerations vary for different prediction tasks. For instance, in the case of rigid body docking methods, having a similar protein in train and test may not be considered leakage if the binding pocket location, conformation and/or pocket interactions with a ligand are sufficiently different. This allows us to evaluate the common use-case of docking a different ligand into a known drug target. However, for co-folding tasks, having such train-test pairs could potentially overestimate model performance as predicted protein structure may contribute more to commonly used accuracy scores than the ligand pose. Likewise, for pocket conditioned ligand generative tasks, similarity between ligand structure and pocket interactions can be expected to contribute to leakage more than receptor sequence similarity. Figure A1 illustrates that using PLINDER similarity annotations, the test and validation set can be further stratified into

task-specific subsets. These make the resource suitable for critical evaluation of various task-specific methods based on novel proteins, ligands, pockets and protein-ligand interactions. This also include the possible intersections that provide a universal testing set.

Our splitting algorithm is configurable by a set of graphs G, each defined on a specific similarity metric, threshold, and a neighbor depth (D) determining the maximum length of the shortest path between two systems to constitute leakage. The $pass\_quality()$ function decides whether a system has high enough experimental quality (see Table A2) to be considered part of the test set. The minimum neighbors m helps avoid singletons or sparsely connected potentially unrealistic systems in the test set, while the maximum neighbors M puts a cap on the number of systems removed from the proto-train set by one test system, to maintain an acceptable training set size. Test set redundancy is limited by allowing only n number of representatives from each component cluster (for a given similarity metric and threshold) to be retained.

Apart from leakage count, we also prioritize test representatives based on the presence of systems within congeneric matched molecular series (MMS, see Appendix A.3), and the number of linked *apo* and predicted structures. For systems in test which are part of a congeneric MMS, all members of that series passing quality criteria are moved to test, and the corresponding leaked systems are removed from proto-train. The obtained proto-train set is further split into training and validation sets based on random 90/10 split of component clusters for a given metric and threshold (`pocket_shared` ≥ 50 weak components was used for the splits presented in this manuscript). The algorithm was applied with the four configurations listed in Table A10 on all PLINDER *holo* systems. We select one of the configurations most applicable to blind-docking (configuration 1) for re-training DiffDock to study the effect of leakage on model performance.

Fraction of leaked systems: For a given train-test split,

DATASET	PLINDER	PDBBIND	DOCKGEN
SYSTEMS	449,383	30,337	41,791
PDB IDS	110,791	19,007	16,881
PASS QUALITY	113,498	10,818	19,355
RECEPTORS	74,256	5,425	7,961
SMILES	51,573	15,279	91,74
CCD CODES	46,988	15,064	9,164
CATH	1,641	649	603
SCOP2B	11,154	2,423	2,817
ECOD T NAME	1,332	528	478
ECOD T ID	4,458	1,444	1,513
PROTEIN KINASE	297	184	174
KINASE INHIBITORS	48,064	4,682	5,605
APO LINKED	98,473	-	-
AFDB LINKED	205,300	-	-

Table 1. **Protein-ligand interaction dataset comparisons.** Only *holo* systems are listed for PLINDER. See Appendix A.4 for PDBBind (v2020) and DockGen mapping. "Pass quality" = systems passing the criteria listed in Table A2. "Receptors" = unique weakly connected components of 100% `protein_fident_global`. "Kinase inhibitors" = systems where a ligand is present in the kinase inhibitors list (Kanev et al., 2020). "Apo linked" and "AFDB linked" = systems linked to one or more *apo* or AFDB structure respectively, as described in Appendix A.2.

similarity metric and threshold, we find the fraction of test systems having at least one connection (an edge with similarity ≥ threshold for that metric) with the train set (also applied to validation vs. test and train vs. PoseBusters).

Since DiffDock is designed for single ligand docking, we focused on *holo* PLI systems involving only a single ligand and selected one system for each unique PDB ID, CCD code combination, yielding 106,745 systems across 35,255 unique ligand SMILES, referred to as PLINDER-NR (non-redundant) for DiffDock training. Split configuration 1 (with G as `pocket_lddt>50`) applied to the PLINDER-NR set is referred to as PLINDER-PL50. We also created a time-based split (PLINDER-TIME), and an ECOD topology-based split (PLINDER-ECOD), both on PLINDER-NR, to compare against PLINDER-PL50 (see Appendix D for more details). PDB IDs in PoseBusters (Buttenschoen et al., 2024) are removed from the training, validation, and test sets in all three splits to evaluate DiffDock model performance on PoseBusters. DiffDock was retrained on the three splits as described in Appendix E.

3. Results

3.1. PLINDER in numbers

At the time of writing of this article, PLINDER contains 1,344,214 PLI systems extracted from 162,978 PDB entries of which 449,383 are *holo* systems (with the remaining consisting of 573,169 systems with common experimental artifacts, 318,060 ion systems, and 3,602 systems con-

taining more than five protein and/or ligand chains, see Appendix A.1 for system classification). Within the *holo* systems, 26% have more than one ligand, 25% have more than one interacting protein chain, and 34% of systems determined by X-ray diffraction pass the X-ray high quality criteria listed in Table A2. As the curation workflow operates on the entire PDB, the collection and labelling of *holo* systems allowed us to simultaneously identify 564,240 PDB chains as being *apo*. Thus, PLINDER also provides an automatically curated dataset of *apo* chains with no detectable ligand interactions (except for artifacts or ions). Table 1 shows how PLINDER compares to the commonly used PDB-Bind (Wang et al., 2005) and DockGen datasets (Corso et al., 2024). Each system in PLINDER has over 500 annotations across the categories listed in Appendix A.

Of the 615,932 ligands in *holo* systems covering 46,988 unique CCD codes, 233,760 (37%) pass the Lipinski Ro5 criteria, 146,444 (23%) have a covalent linkage, 122,741 (19%) are cofactors, 105,836 (17%) are oligo-saccharides, -nucleotides or -peptides, and 55,987 (9%) are fragments. 15,383 systems are part of 2,117 congeneric MMS, each with at least three ligands containing a common core.

3.2. PLINDER splits

As shown in Table 2, the PLINDER-PL50 split exhibits the lowest leakage levels between training and test sets compared to PLINDER-TIME and PLINDER-ECOD. The `pocket_lddt` graph used for splitting eliminates edges between train and test for this metric at threshold above 50%, but also effectively removes most connections based on interactions, pocket location, and protein sequence similarity. Although similar ligands appear in both sets, they bind to different protein pockets which forms an acceptable test-case for the rigid-body docking task and method being assessed.

The PLINDER-ECOD split, despite lower leakage than PLINDER-TIME, reveals issues with incomplete domain annotations. In this case, as systems with no available ECOD annotations were chosen for test, many of these do possess the same domains and pockets seen in the training set. The analogous DockGen split demonstrates that a careful and complete assignment of ECOD domains can reduce leakage but restricts the data that can be assigned and still relies on manual curation efforts.

The large PLINDER dataset size also ensures high diversity sets irrespective of splitting strategy. All PLINDER-PL50 test systems meet high-quality criteria by design, contrasting with 21% and 19% for PLINDER-ECOD and PLINDER-TIME, ensuring reliable ground truth. Table 2 also compares the numbers of train, validation and test systems across the different splits demonstrating our capabilities of creating PLINDER-PL50 dataset-split with a high quality test set con-
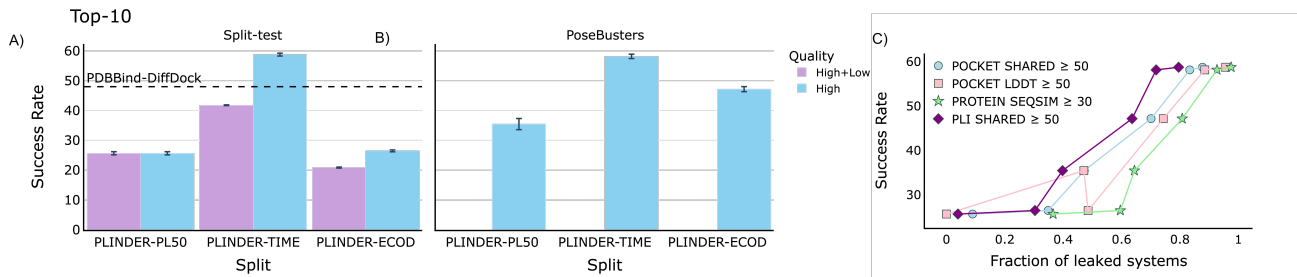
Figure 2. **DiffDock performance**. Success rate as the percentage of test systems with at least one pose with RMSD <2 Å from reference in the Top-10 poses when trained of different training sets and tested on: **A)** corresponding test sets, and **B)** PoseBusters set. **C)** Relationship between DiffDock success rate (high quality test sets) from A) and B) and their fraction of leaked systems as reported in Table A11.

Table 2. Dataset train vs. test split/PoseBusters fraction of leaked systems

SPLIT SET	PLI SHARED ≥ 50	POCKET LDDT ≥ 50	POCKET SHARED ≥ 50	PROTEIN GLOBAL LDDT ≥ 50	PROTEIN SEQSIM ≥ 30	LIGAND SIMILARITY ≥ 30	NO. TRAIN / VAL / TEST	TEST PASS QUALITY%
				VS. TEST SET				
PDBBIND-ORIGINAL	0.91	1.00	1.00	1.00	1.00	0.62	22,365 / 7,549 / 423	50.12
PDBBIND-DIFFDOCK	0.43	0.76	0.73	0.76	0.80	**0.43**	25,442 / 1,570 / 236	22.46
DOCKGEN	0.04	0.08	**0.05**	0.08	**0.18**	0.64	40,916 / 285 / 590	50.00
PDBBIND-LP	0.77	0.87	0.86	0.89	0.94	0.40	18,152 / 3,906 / 7,265	40.37
PLINDER-TIME	0.80	0.96	0.88	0.95	0.98	0.54	76,950 / 11,392 / 11,412	19.28
PLINDER-ECOD	0.30	0.49	0.35	0.49	0.60	0.52	77,411 / 10,169 / 12,174	20.81
PLINDER-PL50	**0.04**	**0.00**	0.09	**0.01**	0.37	0.58	57,602 / 3,453 / 3,729	**100.00**
				VS. POSEBUSTERS				
PDBBIND-DIFFDOCK	0.52	0.69	0.65	0.70	0.78	**0.59**	25,442 / 1,570 / 308	100.00
PLINDER-TIME	0.72	0.88	0.83	0.88	0.93	0.66	76,950 / 11,392 / 308	100.00
PLINDER-ECOD	0.64	0.74	0.70	0.75	0.81	0.65	77,411 / 10,169 / 308	100.00
PLINDER-PL50	**0.40**	**0.47**	**0.47**	**0.48**	**0.64**	0.64	57,602 / 3,453 / 308	100.00

Note that the 41,961 PLINDER-NR systems are removed from the PLINDER-PL50 split by the splitting algorithm to avoid leakage.

taining ten times more complexes than the commonly used PoseBusters set while still maintaining low leakage to the corresponding training set.

3.3. DiffDock performance on different splits

DiffDock was re-trained using NVIDIA BioNeMo (bio) on PLINDER-PL50, PLINDER-ECOD and PLINDER-TIME splits as described in Appendix E. Its performance was evaluated against corresponding test sets, and the standardized PoseBusters benchmark set. All evaluations utilize single A100 GPU inference configurations. Inference protocols involve generating poses of the ligand on a protein and attempting to identify the protein pocket and corresponding ligand configuration from the ground truth test set. Poses are ranked by a confidence model pre-trained as previously described by Corso et al. (2023), and an RMSD is calculated for each pose. Because we trained new score models but used a pre-existing confidence model, the Top-1 pose selection may be erroneous. Therefore, we generate 10 poses, and report Top-1 and Top-10 poses that have RMSD <2Å. The Top-1 pose will be a selection from the unoptimized confidence model, while the Top-10 pose considers the aggregate likelihood of all generated poses, thereby mitigating

the influence of the confidence model. This discrepancy in reported success underscores the necessity of optimizing the confidence model for accurate reporting.

In Figure 2 and Table A12, we present the reported accuracy of our newly trained DiffDock models defined by the training sets in PLINDER-TIME, PLINDER-ECOD, and PLINDER-PL50. On the PoseBusters benchmark set, the baseline Top-1 performance reported for DiffDock trained on the PDBBind-DiffDock split is 38% (Corso et al., 2024). Simply increasing the volume of data without modifying the architecture or considering leakage boosts performance to 47.8% and 58.2% for Top-1 and Top-10 respectively, highlighting the critical role of training set size and diversity in the accuracy of deep learning models. However, with more principled splitting strategies in PLINDER-PL50 and PLINDER-ECOD in which the test set has less information leakage to the training set, we observe a corresponding decrease in accuracy to the 15-18% range (21-26% for Top-10).

We posited that test set quality significantly impacts measured performance. As shown in Figure 2A and Appendix Table A12, DiffDock's performance drops from 45.2% to 29.2% and from 19% to 14.7% for PLINDER-Time and PLINDER-ECOD respectively, when lower quality systems are

added to the test sets. Figure 2C reveals a linear relationship between the fraction of leaked test systems for different metrics and DiffDock performance: for most metrics higher leakage correlates with inflated apparent accuracy (success rate for Top-10 poses against high-quality test). We explore this relationship in more detail in Appendix F. Our quantifiable evidence validates the longstanding intuition regarding the importance of different similarity metrics in de-leaking.

4. Dataset and code availability and updates

Our automated curation workflow enables reproducible periodic updates. For each system, apart from annotations, we provide incremental additions to the protein similarity and ligand similarity datasets for comparative queries, and assign clusters directly based on the new similarity data. On a semi-annual basis, new systems will be consolidated into the existing similarity datasets and clustering will be re-run from scratch and released as a new version. The dataset itself is made available to the public with a CC-BY 4.0 license and hosted on a Google Cloud Storage bucket. The schema of the available dataset will be updated as changes are made and a document describing the draft schema is available here.

The PLINDER source code is Apache 2.0 licensed and can be downloaded at https://github.com/aivant/plinder. Appendix C describes the engineering and software choices which allowed fast and efficient dataset curation and graph querying. Apart from dataset curation, we provide software to evaluate predictions of protein-ligand complexes of any size against reference PLINDER systems using a range of accuracy metrics for ligand (RMSD, lDDT-PLI, PoseBusters), pocket (lDDT-LP), and protein (lDDT, oligomeric scores) levels (Biasini et al., 2013; Studer et al., 2023; Robin et al., 2023; Buttenschoen et al., 2024). In the near future, we plan to release software supporting efficient data loading and diversity sampling of PLINDER, and the PLINDER-2024 split with stratified validation and test sets to make PLINDER readily accessible for the machine learning community.

5. Current limitations and future directions

As the global scientific community continues to generate new experimental data, this work, too, reports an on-going effort to provide the most comprehensive resource for methods in the field of protein-ligand interaction prediction.

We are working towards additional data annotations, such as classical docking scores, cross-docking scores, measured and predicted binding affinities, cryptic pocket and promiscuous ligand labels, to prioritize and stratify test sets with varying properties and auxiliary task labels. We are exploring data augmentation strategies to increase the diversity of interactions, pockets, and folds covered using experi-

mental structures without ligands (Corso et al., 2024) and prediction methods (Voitsitskyi et al., 2024), for which our interaction and leakage detection algorithms are already applicable. While the current release links only a single AlphaFold model to each system, we will make use of the redundancy within UniProt to link multiple predicted structures from the AlphaFold Database to each system. As we observed cases where PLIP failed to detect high similarity between near-identical pockets, we will also explore alternative protein-ligand interaction profilers for curating PLI systems. Our focus on filtering high-quality test systems favours smaller molecules and may underrepresent protein or ligand classes for which only low quality structures are available. Ideally, atom-level weighting would be used in accuracy metrics instead, to be explored in future projects. In addition, while we only utilize quality information for X-ray structures, validation reports for electron microscopy structures now include per-residue Q-scores (Pintilie et al., 2020), which could be incorporated into similar criteria.

To enable a fair assessment of methodological advances we plan to add a leaderboard for commonly adopted methods trained and tested on PLINDER datasets. This will include models trained on the full PLINDER data split, including diversity sampled redundant and augmented systems beyond the subsets described for DiffDock training in this manuscript. We also aim to cover more realistic assessment scenarios of cross-docking or predicting poses within *apo* and predicted receptor structures, with predicted pockets stratified by the extent of conformational change.

6. Conclusion

We present PLINDER a large, comprehensive and automated dataset resource for protein-ligand interactions. We demonstrate the value in scalable similarity measures between protein-ligand complexes and a splitting algorithm that prioritises test set quality and low information leakage. By retraining DiffDock on various splits, we show that our methods and results provide a solid foundation for dataset generation, as well as measuring and addressing both quality and dataset leakage in a quantitative and tunable manner.

7. Acknowledgements

References

Argo Workflow (v3.5.8). https://github.com/argoproj.

NVIDIA BioNeMo (v1.4). https://www.nvidia.com/en-us/clara/bionemo.

Kubernetes (v1.30). https://kubernetes.io/.

Metaflow (v2.11.15). https://docs.metaflow.org/.

Rdkit: Open-source cheminformatics. https://www.rdkit.org. Accessed: 2024-05-17.

Abramson, J., Adler, J., and etal. Accurate structure prediction of biomolecular interactions with alphafold3. *Nature*, 2024. doi: 10.1038/s41586-024-07487-w. URL https://www.nature.com/articles/s41586-024-07487-w.

Adasme, M. F., Linnemann, K. L., Bolz, S. N., Kaiser, F., Salentin, S., Haupt, V. J., and Schroeder, M. PLIP 2021: expanding the scope of the protein–ligand interaction profiler to DNA and RNA. *Nucleic Acids Research*, 49 (W1):W530–W534, 05 2021. ISSN 0305-1048. doi: 10.1093/nar/gkab294. URL https://doi.org/10.1093/nar/gkab294.

Angriman, E., van der Grinten, A., Hamann, M., Meyerhenke, H., and Penschuck, M. Algorithms for large-scale network analysis and the networkit toolkit. In *Algorithms for Big Data: DFG Priority Program 1736*, pp. 3–20. Springer Nature Switzerland Cham, 2023.

Berman, H., Westbrook, J., Z. Feng, G. Gilliland, T. B., Weissig, H., Shindyalov, I., and Bourne, P. The protein dta bank. *Nucleic Acids Research*, 28:235–242, 2000. doi: doi.org/10.1093/nar/28.1.235. URL https://academic.oup.com/nar/article/28/1/235/2384399.

Biasini, M., Schmidt, T., Bienert, S., Mariani, V., Studer, G., Haas, J., Johner, N., Schenk, A. D., Philippsen, A., and Schwede, T. Openstructure: an integrated software framework for computational structural biology. *Acta Crystallographica Section D: Biological Crystallography*, 69(5):701–709, 2013.

Bickerton, G. R., Paolini, G. V., Besnard, J., Muresan, S., and Hopkins, A. L. Quantifying the chemical beauty of drugs. *Nature chemistry*, 4(2):90–98, 2012.

Buttenschoen, M., Morris, G. M., and Deane, C. M. Posebusters: Ai-based docking methods fail to generate physically valid poses or generalise to novel sequences. *Chem. Sci.*, 15:3130–3139, 2024. doi: 10.1039/D3SC04185A. URL http://dx.doi.org/10.1039/D3SC04185A.

Chawdhury, T. K., Grant, D. J., and Jin, H. Y. Deep2lead: A distributed deep learning application for small molecule lead optimization, 2021. URL https://arxiv.org/abs/2108.05183.

Chen, V. B., Arendall, W. B., Headd, J. J., Keedy, D. A., Immormino, R. M., Kapral, G. J., Murray, L. W., Richardson, J. S., and Richardson, D. C. Molprobity: all-atom structure validation for macromolecular crystallography. *Acta Crystallographica Section D: Biological Crystallography*, 66(1):12–21, 2010.

Cheng, H., Schaeffer, R. D., Liao, Y., Kinch, L. N., and Pei, J. Ecod: An evolutionary classification of protein domains. *PLOS Computational Biology*, 10(12): e1003926, 2014. doi: 10.1371/journal.pcbi.1003926. URL https://journals.plos.org/ploscompbiol/article?id=10.1371/journal.pcbi.1003926.

Choudhary, P., Feng, Z., Berrisford, J., Chao, H., Ikegawa, Y., Peisach, E., Piehl, D. W., Smith, J., Tanweer, A., Varadi, M., Westbrook, J. D., Young, J. Y., Patwardhan, A., Morris, K. L., Hoch, J. C., Kurisu, G., Velankar, S., and Burley, S. K. Pdb nextgen archive: Centralising access to integrated annotations and enriched structural information by the worldwide protein data bank. *bioRxiv*, 2023. doi: 10.1101/2023.10.24.563739. URL https://www.biorxiv.org/content/early/2023/10/27/2023.10.24.563739.full.pdf.

Consortium, U. Uniprot: a worldwide hub of protein knowledge. *Nucleic acids research*, 47(D1):D506–D515, 2019.

Corso, G., Stärk, H., Jing, B., Barzilay, R., and Jaakkola, T. Diffdock: Diffusion steps, twists, and turns for molecular docking, 2023. URL https://arxiv.org/abs/2210.01776.

Corso, G., Deng, A., Fry, B., Polizzi, N., Barzilay, R., and Jaakkola, T. Deep confident steps to new pockets: Strategies for docking generalization, 2024. URL https://arxiv.org/abs/2402.18396.

Dauparas, J., Lee, G. R., Pecoraro, R., An, L., Anishchenko, I., Glasscock, C., and Baker, D. Atomic context-conditioned protein sequence design using ligandmpnn. *bioRxiv*, 2023. doi: 10.1101/2023.12.22.573103. URL https://www.biorxiv.org/content/early/2023/12/23/2023.12.22.573103.

Dutta, S., Dimitropoulos, D., Feng, Z., Persikova, I., Sen, S., Shao, C., Westbrook, J., Young, J., Zhuravleva, M. A., Kleywegt, G. J., and Berman, H. M. Improving the representation of peptide-like inhibitor and antibiotic molecules in the protein data bank. *Biopolymers*, 101(6):659–668, 2014. doi: 10.1002/bip.

22434. URL https://onlinelibrary.wiley.com/doi/abs/10.1002/bip.22434.

Jasial, S., Hu, Y., Vogt, M., and Bajorath, J. Activity-relevant similarity values for fingerprints and implications for similarity searching [version 2; peer review: 3 approved]. *F1000Research*, 5(591), 2016. doi: 10.12688/f1000research.8357.2.

Jumper, J., Evans, R., Pritzel, A., Green, T., Figurnov, M., Ronneberger, O., Tunyasuvunakool, K., Bates, R., Žídek, A., Potapenko, A., Bridgland, A., Meyer, C., Kohl, S. A. A., Ballard, A. J., Cowie, A., Romera-Paredes, B., Nikolov, S., Jain, R., Adler, J., Back, T., Petersen, S., Reiman, D., Clancy, E., Zielinski, M., Steinegger, M., Pacholska, M., Berghammer, T., Bodenstein, S., Silver, D., Vinyals, O., Senior, A. W., Kavukcuoglu, K., Kohli, P., and Hassabis, D. Highly accurate protein structure prediction with alphafold. *Nature*, 596(7873):583–589, 2021. doi: 10.1038/s41586-021-03819-2. URL https://www.nature.com/articles/s41586-021-03819-2.

Kanev, G. K., de Graaf, C., Westerman, B. A., de Esch, I. J. P., and Kooistra, A. J. KLIFS: an overhaul after the first 5 years of supporting kinase research. *Nucleic Acids Research*, 49(D1):D562–D569, 10 2020. ISSN 0305-1048. doi: 10.1093/nar/gkaa895. URL https://doi.org/10.1093/nar/gkaa895.

Krishna, R., Wang, J., Ahern, W., Sturmfels, P., Venkatesh, P., Kalvet, I., Lee, G. R., Morey-Burrows, F. S., Anishchenko, I., Humphreys, I. R., McHugh, R., Vafeados, D., Li, X., Sutherland, G. A., Hitchcock, A., Hunter, C. N., Kang, A., Brackenbrough, E., Bera, A. K., Baek, M., DiMaio, F., and Baker, D. Generalized biomolecular modeling and design with rosettafold all-atom. *Science*, 384(6693):eadl2528, 2024. doi: 10.1126/science.adl2528. URL https://www.science.org/doi/abs/10.1126/science.adl2528.

Leemann, M., Sagasta, A., Eberhardt, J., Schwede, T., Robin, X., and Durairaj, J. Automated benchmarking of combined protein structure and ligand conformation prediction. *Proteins: Structure, Function, and Bioinformatics*, 91(12):1912–1924, 2023.

Li, J., Guan, X., Zhang, O., Sun, K., Wang, Y., Bagni, D., and Head-Gordon, T. Leak proof pdbbind: A re-organized dataset of protein-ligand complexes for more generalizable binding affinity prediction, 2024. URL https://arxiv.org/html/2308.09639v2.

Liu, Z., Li, Y., Han, L., Li, J., Liu, J., Zhao, Z., Nie, W., Liu, Y., and Wang, R. Pdb-wide collection of binding data: current status of the pdbbind database. *Bioinformatics*, 31(3):405–412, 2015.

Lu, W., Wu, Q., Zhang, J., Rao, J., Li, C., and Zheng, S. Tankbind: Trigonometry-aware neural networks for drug-protein binding structure prediction. *bioRxiv*, 2022. doi: 10.1101/2022.06.06.495043. URL https://www.biorxiv.org/content/early/2022/06/06/2022.06.06.495043.

Mistry, J., Chuguransky, S., Williams, L., Qureshi, M., Salazar, G. A., Sonnhammer, E. L., Tosatto, S. C., Paladin, L., Raj, S., Richardson, L. J., et al. Pfam: The protein families database in 2021. *Nucleic acids research*, 49(D1):D412–D419, 2021.

Murzin, A. G., Brenner, S. E., Hubbard, T., and Chothia, C. Scop: a structural classification of proteins database for the investigation of sequences and structures. *Journal of molecular biology*, 247(4):536–540, 1995.

O'Boyle, N. M., Morley, C., and Hutchison, G. R. Pybel: a python wrapper for the openbabel cheminformatics toolkit. *Chemistry Central Journal*, 2:5, 12 2008. ISSN 1752-153X. doi: 10.1186/1752-153X-2-5. URL https://bmcchem.biomedcentral.com/articles/10.1186/1752-153X-2-5.

Orengo, C. A., Michie, A. D., Jones, S., Jones, D. T., Swindells, M. B., and Thornton, J. M. Cath–a hierarchic classification of protein domain structures. *Structure*, 5(8):1093–1109, 1997.

Pintilie, G., Zhang, K., Su, Z., Li, S., Schmid, M. F., and Chiu, W. Measurement of atom resolvability in cryo-em maps with q-scores. *Nature methods*, 17(3):328–334, 2020.

Plainer, M., Toth, M., Dobers, S., Stark, H., Corso, G., Marquet, C., and Barzilay, R. Diffdock-pocket: Diffusion for pocket-level docking with sidechain flexibility. In *NeurIPS 2023 Workshop on New Frontiers of AI for Drug Discovery and Development*, 2023. URL https://openreview.net/forum?id=5Wt7qNRc5u.

Qiao, Z., Nie, W., Vahdat, A., III, T. F. M., and Anandkumar, A. State-specific protein–ligand complex structure prediction with a multiscale deep generative model. *Nature Machine Intelligence*, 6:195–208, 2024. doi: 10.1038/s42256-024-00792-z. URL https://www.nature.com/articles/s42256-024-00792-z.

Raasveldt, M. and Muehleisen, H. DuckDB. URL https://github.com/duckdb/duckdb.

Robin, X., Studer, G., Durairaj, J., Eberhardt, J., Schwede, T., and Walters, W. P. Assessment of protein–ligand complexes in casp15. *Proteins: Structure, Function, and Bioinformatics*, 91(12):1811–1821, 2023.

Schneuing, A., Du, Y., Harris, C., Jamasb, A., Igashov, I., Du, W., Blundell, T., Lió, P., Gomes, C., Welling, M., Bronstein, M., and Correia, B. Structure-based drug design with equivariant diffusion models, 2023.

Steinegger, M. and Söding, J. MMseqs2 enables sensitive protein sequence searching for the analysis of massive data sets. *Nature Biotechnology*, 35:1026–1028, 2017. doi: https://doi.org/10.1038/nbt.3988. URL https://www.nature.com/articles/nbt.3988.

Studer, G., Tauriello, G., and Schwede, T. Assessment of the assessment—all about complexes. *Proteins: Structure, Function, and Bioinformatics*, 91(12):1850–1860, 2023.

Stärk, H., Ganea, O., Pattanaik, L., Barzilay, R., and Jaakkola, T. Equibind: Geometric deep learning for drug binding structure prediction, 2022. URL https://arxiv.org/abs/2202.05146.

Thomas, P. D., Ebert, D., Muruganujan, A., Mushayahama, T., Albou, L.-P., and Mi, H. Panther: Making genome-scale phylogenetics accessible to all. *Protein Science*, 31 (1):8–22, 2022.

van Kempen, M., Kim, S. S., Tumescheit, C., Mirdita, M., Lee, J., Gilchrist, C. L. M., Söding, J., and Steinegger, M. Fast and accurate protein structure search with Foldseek. *Nature Biotechnology*, 42:243–246, 2024. doi: https://doi.org/10.1038/s41587-023-01773-0. URL https://www.nature.com/articles/s41587-023-01773-0.

Varadi, M., Anyango, S., Deshpande, M., Nair, S., Natassia, C., Yordanova, G., Yuan, D., Stroe, O., Wood, G., Laydon, A., Žídek, A., Green, T., Tunyasuvunakool, K., Petersen, S., Jumper, J., Clancy, E., Green, R., Vora, A., Lutfi, M., Figurnov, M., Cowie, A., Hobbs, N., Kohli, P., Kleywegt, G., Birney, E., Hassabis, D., and Velankar, S. Alphafold protein structure database: massively expanding the structural coverage of protein-sequence space with high-accuracy models. *Nucleic Acids Research*, 50(D1): D439–D444, 2022. doi: 10.1093/nar/gkab1061. URL https://doi.org/10.1093/nar/gkab1061.

Voitsitskyi, T., Yesylevskyy, S., Bdzhola, V., Stratiichuk, R., Koleiev, I., Ostrovsky, Z., Vozniak, V., Khropachov, I., Henitsoi, P., Popryho, L., Zhytar, R., Nafiiev, A., and Starosyla, S. Artidock: fast and accurate machine learning approach to protein-ligand docking based on multimodal data augmentation. *bioRxiv*, 2024. doi: 10.1101/2024.03.14.585019. URL https://www.biorxiv.org/content/early/2024/03/16/2024.03.14.585019.

Wang, R., Fang, X., Lu, Y., Yang, C., and Wang, S. The PDBbind Database: Methodologies and Updates. *Journal of Medicine Chemistry*, 48(12):4111–4119, 2005. doi: 10.1021/jm048957q. URL https://pubs.acs.org/doi/10.1021/jm048957q.

Warren, G. L., Do, T. D., Kelley, B. P., Nicholls, A., and Warren, S. D. Essential considerations for using protein–ligand structures in drug discovery. *Drug Discovery Today*, 17(23-24):1270–1281, 2012.

Westbrook, J. D., Shao, C., Feng, Z., Zhuravleva, M., Velankar, S., and Young, J. The chemical component dictionary: complete descriptions of constituent molecules in experimentally determined 3d macromolecules in the protein data bank. *Bioinformatics*, 31(8):1274–1278, 2015.

Wildman, S. A. and Crippen, G. M. Prediction of physicochemical parameters by atomic contributions. *Journal of chemical information and computer sciences*, 39(5): 868–873, 1999.

Zhang, C., Zhang, X., Freddolino, P. L., and Zhang, Y. BioLiP2: an updated structure database for biologically relevant ligand-protein interactions. *Nucleic acids research*, 52(D1):D404–D412, 2024. doi: 10.1093/nar/gkad630. URL https://academic.oup.com/nar/article/52/D1/D404/7233921.

A. Curation and Annotation

A.1. Ligand and *holo* system annotation

In order to characterize our systems, we identified small-molecules that are not considered PLINDER ligands - artifacts and single (non-hydrogen) atom or ion entities. All entities containing a single atom, excluding basic organic elements C, H, N, O, P, S, were kept as auxiliary entity, which we refer as an "ion", irrespective of its oxidation state (eg. Fe^{2+}, Xe, Cl^-). These entities were considered as part of the pocket, if they were within 4 Å distance from the ligand, but not considered as a ligand (hereafter referred to as "ions"). To enrich for biologically and therapeutically relevant ligands, we further excluded molecules that contain few atoms (less than 2 carbons or less than 5 non-hydrogen atoms), are highly charged (absolute charge more than 2), have long unbranched hydrocarbon linkers (longer than 12), contain unspecified atoms or are common experimental buffer artifacts. The artifact entries were curated based on commonly used artifact definitions (Zhang et al., 2024) and including additional commonly occurring buffer reagents, but excluding biologically relevant co-factors or sugars (eg. NAG). The list used is provided in Table A4. The ligand inclusion criteria is summarized in Table A3, if the molecule does not pass the criteria - it is labelled as an "artifact". All PLI systems which have at least one ligand that passes the curation criteria form our dataset of *holo* systems.

Each detected ligand was assigned a unique canonical SMILES. For single residue ligands we used the Chemical Component Dictionary (CCD) (Westbrook et al., 2015) to identify the SMILES. If the ligand name was not present in the CCD or it consisted of multiple residues, we used the resolved SMILES value from PLIP that was further standardized via RDKit canonicalization. We then used the canonical SMILES to calculate ligand descriptors for Lipinski criteria and other commonly used metrics such as the quantitative estimate of drug-likeness (QED) (Bickerton et al., 2012). Finally, the SMILES were used to assign bond orders to resolved ligand atoms. When some atoms were missing in the resolved structure, we used substructure matching to identify the relevant molecular fragments to assign the bond orders. In case of failure to assign bond orders from SMILES, we used OpenBabel (O'Boyle et al., 2008) to assign the bond orders. Despite our best efforts not all ligands were successfully processed by RDKit. In Table A5 we report the numbers for PLINDER total and RDKit-processable ligand SMILES. Note that these numbers also include ions and artifacts not counted in Table 1.

Table A6 provides and overview for numbers of protein and ligand chains per *holo* system in PLINDER dataset.

A.2. *Apo*, predicted and cross-docking structures

Each system is associated where possible to related (1) *apo* chains, (2) predicted structures from the AlphaFold database (Varadi et al., 2022; Jumper et al., 2021) and (3) other *holo* systems.

Apo protein chains within each PDB entry are defined as those with a different entity identifier to any protein chain in that entry participating in a *holo* system. These are collected across the entire PDB to form the database of *apo* chains. Similarly, a database of predicted structures is constructed using the sequences and AFDB models of all UniProt IDs associated with PDB structures. A similar Foldseek and MM-seqs search as described in Section 2.2 is performed for the *holo* systems against these two databases with min_seq_id set to 0.9 and minimum query coverage set to 0.9, to calculate all the protein scores, as well as the `pocket_lddt` and `pocket_identity` scores (Note that the remaining scores cannot be calculated as they depend on the presence of a ligand and binding pocket in the target). Cross-docking structures are instead obtained for each system using the similarities already calculated in 2.2. The *apo*, predicted and cross-docking hits are further restricted with a filter of 95% `pocket_identity`.

Each linked structure is superposed to the corresponding system and additional metrics are calculated based on transplanting the ligand from the system to the linked structure. These include the RMSD of the superposition as well as the lDDT-LP, lDDT-PLI (Robin et al., 2023) and PoseBusters checks (Buttenschoen et al., 2024) of the transplanted ligand.

A.3. Matched molecular series

To enable evaluation of lead optimization use-cases, we detected PLI systems containing matched molecular series (MMS), where the ligands in the set all contain the same constant core and each pair within the set only differ by a single chemical transformation. This allows evaluating the performance in use-cases, where both pockets and some members of a chemical series are known and methods are used to prioritize changes to this series that optimize binding. This is a key part of typical lead optimization stages of drug development, and this annotation allows for fair evaluation of methods that make use of this prior knowledge available at inference time.

Using all the annotated ligands, we generated the mmpdb index using default parameters. This index maps ligands that are matched molecular pairs to their shared core scaffold. We dropped scaffolds which were fragmented or contained less than 5 atoms. Systems with pockets in the same 95% `protein_identity` and 100% `pocket_identity_shared` strong components con-

Category	Annotations
Identifiers	PDB ID, biounit, interacting protein chains and residue numbers, ligand chains
Entry information	Release date, oligomeric state, determination method, keywords, pH
System information	System type (*holo*, artifact, ion, see Appendix A.1), CCD code, unique CCD code (de-duplicated for identical molecules with different CCD codes), canonical SMILES, resolved SMILES
Ligand properties	Molecular weight, Wildman-Crippen ClogP (Wildman & Crippen, 1999), hydrogen bond donor and acceptor counts, number of rings, number of heavy atoms, QED (Bickerton et al., 2012), covalent bonds, passing Lipinski's rule of five (Ro5) criteria, detected as fragment, detected as oligo-peptide, -saccharide or -nucleotide, presence in cofactor list, presence in artifact list, presence in list of kinase inhibitors (Kanev et al., 2020), BIRD ID (Dutta et al., 2014), detected PLIP interactions (Adasme et al., 2021), PoseBusters checks (Buttenschoen et al., 2024)
Protein properties	CATH (Orengo et al., 1997), ECOD (Cheng et al., 2014), SCOP (Murzin et al., 1995), Pfam (Mistry et al., 2021), UniProt (Consortium, 2019), Kinase (Kanev et al., 2020), PANTHER (Thomas et al., 2022) for each protein chain in the entry and also aggregated to the system pocket
Entry quality	Resolution, R, R_{free}, clash score, % Ramachandran outliers, % rotamer outliers, % RSRZ outliers, data completenessMolProbity score (Chen et al., 2010)
Per-residue quality	RSR, RSCC, RSRZ,occupancy, missing/resolved atom counts, outliers (clash, geometry, density, chirality) and alternative configuration count. Per-residue quality metrics are also aggregated across ligands, pockets, and chains.
Similarity clusters	Protein, pocket, PLI, and ligand-level components at thresholds of 50%, 70%, 95% and 100% for metrics listed in Appendix B
Matched molecular series	Congeneric series IDs, core scaffolds and transformations, see Appendix A.3
Linked structures (*apo*, AFDB)	Associated similarity scores, CIF files superposed to each *holo* system, superposition RMSD, lDDT-LP, lDDT-PLI (Robin et al., 2023), and PoseBusters results based on transplanted ligand, see Appendix A.2
System files	MMCIF and PDB files of all ligand chains, interacting protein chains and interacting waters extracted from the biounit. SDF files of each ligand chain. Note: chains are renamed for PDB format.

Table A1. **Annotations available per system**. Annotation availability is indicated with a copper color scheme, where light orange is zero availability, **brown** is 50% availability and **black** is available in all systems. For boolean annotations such as "presence in cofactor list", the color indicates how many systems have the annotation as True.

Table A2. X-ray high quality criteria for PLI systems, based on a combination of relevant previously defined criteria (Warren et al., 2012; Leemann et al., 2023; Buttenschoen et al., 2024).

PROPERTY	TEST VALUE
ENTRY	
RESOLUTION	≤ 3.5
R-FACTOR	≤ 0.4
R_{free}	≤ 0.45
$R - R_{free}$	≤ 0.05
LIGAND AND POCKET	
NO UNRESOLVED HEAVY ATOMS	TRUE
NO ALTERNATIVE CONFIGURATIONS	TRUE
AVERAGE OCCUPANCY	≥ 0.8
AVERAGE RSCC	≥ 0.8
AVERAGE RSR	≤ 0.3
LIGAND	
NO CLASH OUTLIERS	TRUE

Table A3. Non-artifact ligand classification criteria

PROPERTY	VALUE
IS A SINGLE ATOM (ION)	FALSE
NON-H ATOM COUNT	> 5
C ATOM COUNT	> 2
ABSOLUTE CHARGE	≤ 2
UNBRANCHED HYDROCARBON LINKER LENGTH	≤ 12
UNSPECIFIED ATOM (*) COUNT	0
CCD CODE (OR SYNONYM) IN TABLE A4	FALSE

A.4. Comparison with other PLI datasets

We selected PDBBind (Wang et al., 2005), and Dock-Gen (Corso et al., 2024) to compare PLINDER against PLI datasets that have previously been used for training and evaluation of deep learning methods. These datasets are mapped to PLINDER using a combination of PDB IDs and CCD codes, with the first biounit containing the ligand considered for PDBBind and specified biounit identifiers for DockGen.

taining ligands sharing the same scaffold are collected into congeneric MMS.

Table A4. CCD codes of ligands that are treated as artifacts

02U, 12P, 13P, 144, 15P, 16P, 1EM, 1PE, 1PG, 1PS, 2DP, 2JC, 2NV, 2OP, 2PE, 32M, 33O, 3HR, 3PG, 3SY, 3V3, 543, 6JZ, 6PE, 7E8, 7E9, 7I7, 7N5, 7PE, 7PG, 7PH, 90A, 9FO, 9JE, 9YU, AAE, ABA, AE3, AE4, AGA, AKR, AUC, B3H, B3P, B4T, B4X, BAM, BCN, BDN, BE7, BEN, BET, BEZ, BGL, BHG, BNG, BNZ, BOG, BTB, BU1, BXC, C10, C14, C8E, CAC, CAD, CAQ, CD4, CE1, CE9, CHT, CIT, CN3, CN6, CPS, CXE, CXS, D10, D12, D1D, D22, DAO, DD9, DDQ, DDR, DEP, DET, DHB, DHJ, DIO, DKA, DMF, DMI, DMR, DOX, DPG, DR6, DRE, DTD, DTT, DTU, DTV, E4N, EAP, EEE, EPE, ETE, ETF, ETX, F09, F4R, FJO, FTT, FW5, GLV, GOL, GVT, GYF, HAE, HAI, HCA, HCS, HED, HEX, HEZ, HP6, HSG, HSH, HT3, HTG, HTH, HTO, HZA, I3C, ICT, IHP, IHS, IMD, IPH, JDJ, K12, KDO, L1P, L2C, L2P, L3P, L4P, LAC, LDA, LI1, LMR, LMT, LMU, LUT, M2M, MAC, MAE, MB3, MBN, MBO, MC3, ME2, MEG, MES, MLA, MLI, MLT, MPD, MPO, MRD, MSE, MYR, N8E, NBN, NET, NEX, NHE, O4B, OCT, OES, OGA, OP2, OTE, OXM, P03, P15, P1O, P22, P25, P2K, P33, P3G, P4C, P4G, P4K, P6G, PA8, PC8, PD7, PE3, PE4, PE5, PE6, PE7, PE8, PEG, PEP, PEU, PEX, PG0, PG4, PG5, PG6, PG8, PGE, PGF, PGO, PGR, PHB, PHQ, PL9, PLC, PMS, PPI, PQ9, PQE, PTD, PUT, PVO, PX2, PX4, QGT, QJE, QLB, RG1, RWB, SAR, SEP, SGM, SIN, SOG, SP5, SPD, SPJ, SPM, SPZ, SQU, SRT, TAM, TAR, TAU, TBU, TCE, TCN, TEA, TFA, THE, TLA, TMA, TOE, TPO, TRD, TRS, UMQ, UND, V1J, VX, XAT, XP4, XPA, XPE, Y69.

Table A5. Ligand annotation overview in PLINDER

Ligand Type	Number of Unique Items
Ligand SMILES	54,089
Ligand RDKit Canonical SMILES	53,543
Ligand CCD Code	48,271

Table A6. Number of protein chains and ligand chains in PLINDER *holo* systems

PROTEIN CHAINS	LIGANDS	SYSTEM IDS
1	1	257836
	2	57312
	3	16854
	4	4508
	5	1417
2	1	62977
	2	25852
	3	5985
	4	2691
	5	809
3	1	7129
	2	2057
	3	1163
	4	312
	5	83
4	1	1347
	2	481
	3	88
	4	126
	5	29
5	1	201
	2	23
	3	6
	4	19
	5	78

Mapping details are shown in Table A7 and Table A8. Systems with annotations in PLINDER that differ from PDBBind or Dockgen are referred to as inconsistent with PLINDER. For example, some ligands labeled as peptides with four amino acids in PDBBind were found to have five or six amino acids in PLINDER, or were identified with entirely different ligand CCD codes. PDB IDs that did not pass the PLINDER processing pipeline are referred to as not in PLINDER. These consist of cases in PDBBind and DockGen containing peptides longer than 11 amino acids, which are not considered as ligands in PLINDER.

B. Similarity measures

B.1. Protein similarity

Foldseek and MMSeqs searches were run on all PDB chains present in all systems (E-value < 0.01, min_seq_id 0.2, max_seqs 5000). The fraction of identical residues and query coverage were saved along with the full query and target alignments. Additionally for Foldseek, alignment lDDT and lDDT scores per aligned residue were saved. These search results are used to define the following protein level similarities for a given alignment, with the highest value being taken for each if both Foldseek and MMSeqs alignments

are found:

- **protein_lddt**: lDDT score
- **protein_identity**: Percentage of identical residues
- **protein_seqsim**: Sequence similarity
- **protein_qcov**: Query coverage
- **protein_lddt_global, protein_identity_global, protein_seqsim_global**: Corresponding similarities multiplied by the query coverage, approximates the value for the global alignment.

For systems with more than one interacting protein chain, greedy chain mapping is performed using the protein_lddt_global score where available and protein_identity_global otherwise.

The protein similarity score ($S_{a,b}$) between systems a and b is then calculated as a weighted mean across the mapped pairs of chains (i, j), with the weight (l_i) defined by the
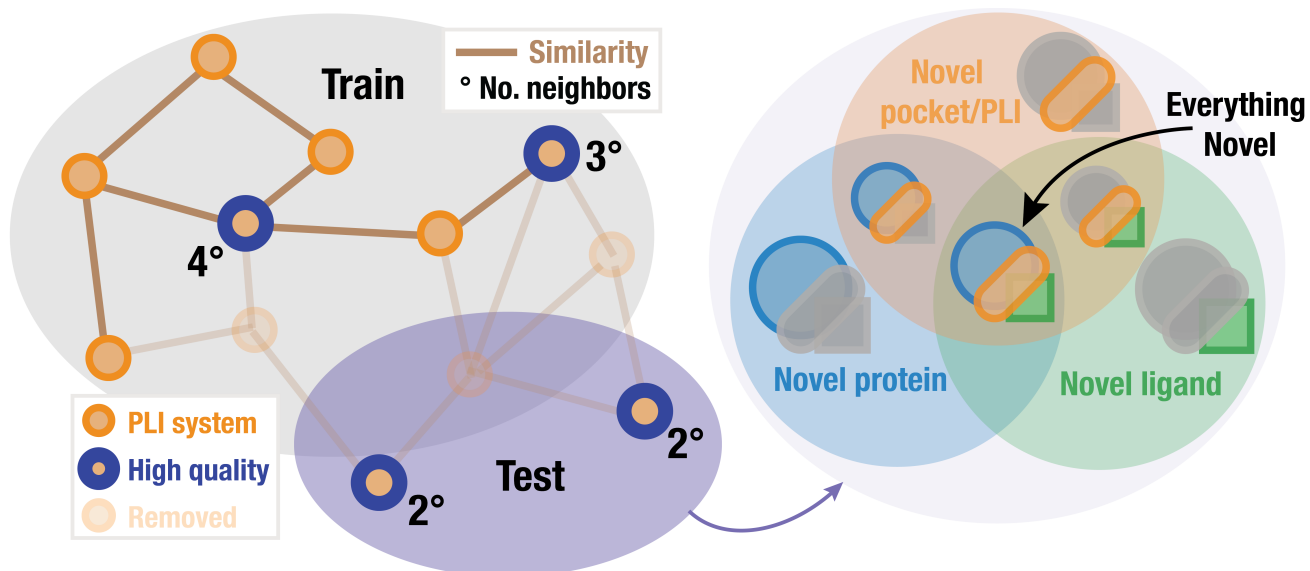
Figure A1. PLINDER test sets can be further stratified into subsets using extensive system similarity annotations. The test and validation sets can be further subsplit into subsets of novel protein, ligand and protein-ligand interaction systems, including their intersections for potential multi-task testing.

Table A7. PDBBind mapping to PLINDER details

PDBBind 2020	
total PDB ID + ligand CCD combinations	19443
total PDB IDs	19443
total ligand CCDs	12930
PDB IDs in PLINDER	19007
PDB IDs + Ligand CCD ID inconsistent with PLINDER	1375
holo systems in PLINDER	28184
ion systems in PLINDER	711
artifact systems in PLINDER	1442
PDB IDs not in PLINDER	436
systems in PLINDER	30337

Table A8. DockGen mapping to PLINDER details

DockGen	
total PDB ID + Biounit ID + Ligand CCD combination	26007
total PDB IDs	18504
total Ligand CCD	9338
PDB IDs in PLINDER	18391
PDB IDs + Ligand CCD ID inconsistent with PLINDER	1510
holo systems in PLINDER	37656
ion systems in PLINDER	3212
artifact systems in PLINDER	923
PDB IDs not in PLINDER	113
systems in PLINDER	41791

length of each query protein chain.

$$S_{a,b} = \frac{\Sigma_{i \in a}(l_i . S_{i,j})}{\Sigma_{i \in a} l_i}$$

B.2. Pocket similarity

The alignment results and chain mappings obtained from protein similarity calculation are combined with information about the binding pocket, i.e residues in proximity to the ligand, to define the following pocket level scores:

- **pocket_shared** The percentage of shared and aligned binding pocket residues

$$\frac{|B_a \cap \text{Aligned}_{a \to b}(B_b)|}{|B_a|}$$

where the binding pocket residues of the query system a (B_a) are only considered if the corresponding aligned residue in the target system b, $\text{Aligned}_{a \to b}$, is also in B_b.

- **pocket_identity** The percentage of identical residues in the query binding pocket

$$\frac{\Sigma_{n \in B_a} B_a{}^n = \text{Aligned}_{a \to b}^n}{|B_a|}$$

- **pocket_identity_shared** The percentage of shared, aligned and identical binding pocket residues

$$\frac{\Sigma_{n \in (B_a \cap \text{Aligned}_{a \to b}(B_b))} B_a{}^n = \text{Aligned}_{a \to b}^n}{|B_a|}$$

- **pocket_lddt** The mean lDDT of query binding pocket residues

$$\frac{\Sigma_{n \in B_a} \text{lDDT}_n}{|B_a|}$$

- **pocket_lddt_shared** The mean lDDT of shared and aligned binding pocket residues

$$\frac{\Sigma_{n \in (B_a \cap \text{Aligned}_{a \to b}(B_b))} \text{lDDT}_n}{|B_a|}$$

B.3. Protein-ligand interaction similarity

We convert each PLIP interaction into a unique string, defined by the interaction type and type-specific attributes as defined in Table A9.

Table A9. Attributes used to define protein-ligand interaction types

INTERACTION TYPE	ATTRIBUTES
HYDROGEN BONDS	IS PROTEIN THE DONOR?, IS THE BOND WITH A SIDECHAIN?
HYDROPHOBIC	-
SALT BRIDGES	DOES THE PROTEIN CARRY THE POSITIVE CHARGE?
WATER BRIDGES	IS PROTEIN THE DONOR?
π STACKS	STACKING TYPE
π-CATION	DOES THE PROTEIN PROVIDE THE CHARGE?
HALOGEN BONDS	IS THE BOND WITH A SIDECHAIN?
METAL COMPLEXES	METAL TYPE, TARGET TYPE, COORDINATION, GEOMETRY, LOCATION

The collection of hashed PLIP interactions is used to define a weighted Jaccard index:

$$J_w(I_a, I_b) = \frac{\sum \min(a_i, b_i)}{\sum \max(a_i, b_i)}$$

Where I_a and I_b are the multisets of interactions, a_i and b_i are the counts of each unique interaction in I_a and I_b respectively, $\min(a_i, b_i)$ is the minimum count of each interaction found in both sets, and $\max(a_i, b_i)$ is the maximum count of each interaction across both sets.

The **pli_shared** between two systems a and b is then defined by comparing the interactions at each aligning pocket residue:

$$\frac{\Sigma_{n \in (B_a \cap \text{Aligned}_{a \to b}(B_b))} J_w(I_a^n, I_b^n)}{|I_a|}$$

B.4. Ligand similarity

To detect ligand similarity, we generate ECFP4 fingerprints with length of bits 1024 using RDKit (rdk) on ligand SMILES. We then calculated Tanimoto coefficient for each ligand pair. When more than one ligand present in a PLI system, we used the maximum similarity for each individual pair of systems. To be consistent with protein similarity

scores, as well as for storage and querying efficiency, we first ranked all the Tanimoto coefficients and saved only the top 5000 pairs. For potential leakage detection we used the 30% and 50% cutoffs previously reported for ligand based activity enrichment (Jasial et al., 2016).

C. Dataset construction and engineering considerations

The data ingestion and data processing required to produce the complete PLINDER dataset involves large scale orchestration of a non-trivial amount of computational resources. We leverage the metaflow (met) framework to define a directed acyclic graph (DAG) of the work to be completed. This enables us to implement the processing logic in normal python code, and then simply write a metaflow.FlowSpec to distribute the work in a kubernetes (kub) cluster. We promote the FlowSpec to an argo (Arg) workflow template in order to execute the entire end-to-end pipeline in the cloud.

The RCSB rsync API makes it convenient to distribute the initial dataset ingestion along the middle two character codes of PDB IDs. However, the number of entries within a two character code are not evenly distributed, leading to uneven run times, making it a poor choice for distributing other stages in the workflow. For stages such as annotation generation and scoring, we batch chunks of PDB IDs and distribute along these chunks instead. Using either two character code or PDB ID chunks with tunable chunk sizes allows us to choose between simple distribution logic and desired total run time.

Careful consideration of distributing the workload affords the ability to run a majority of the end-to-end pipeline on commodity machines, with few exceptions. The first is for the large foldseek and mmseqs database creation steps, which are vertically scaled on a 96 core machine. Additionally, the cluster generation and splitting steps use up to 100 GB of memory because they require reading a significant portion of the protein similarity dataset into memory in order to construct the graphs.

Downstream stages of the workflow that leverage the similarity and cluster datasets initially suffered from a substantial bottleneck simply reading the data from disk. Converting the data to parquet files and partitioning the data based on commonly applied query filters reduced query times from 30 minutes or more to under 10 minutes. Subsequent adoption of the duckdb(Raasveldt & Muehleisen) embedded database engine with its query optimizer further reduces query times by a factor of up to two to four. Currently, materialization of the data into a data frame is the slowest step for large queries (100 million to 1 billion records). Finally, since duckdb supports standard query language (SQL), it

is possible to push complex aggregations that are currently done in python into the query itself, including cross-dataset joins, further reducing the cost in both time and memory of querying these data.

D. Comparing splitting methods

To evaluate generalizability of deep learning model performance, along with PLINDER the dataset itself, we propose a splitting algorithm 1 which can separate dissimilar protein-ligand interactions, protein and ligands systems into training, validation, test sets while maintaining test set quality and train and test set diversity. We applied this algorithm with four different configurations, listed in Table A10 on the entire PLINDER dataset. For all splits, $m = 2$, $M = 400$, C is defined by the strongly connected components of `pli_shared` ≥ 70, and $n = 5$. The resulting proto-train sets were divided into train and validation sets based on weakly connected components of `pocket_shared` ≥ 50. As shown by the fraction of leaked systems for different metrics and thresholds in Table A10, splitting by different similarity graphs removes leakage for that metric and to varying extents also removes connections based on other metrics. For example, splitting based on the `pocket_shared` ≥ 20 graph (configuration 2) only ensures that train and test systems do have a ligand-binding pocket in the same location. As seen by the resulting fraction of leaked systems for `protein_seqsim` for this configuration, this implies that similar proteins are in train and test (but necessarily with ligands bound in different locations). Similarly, as none of these configurations performed splitting using the ligand similarity graph, similar ligands are in both train and test for all splits. Future efforts will go towards optimizing thresholds and the m and M parameters to obtain a required test-set size, combining different component clusters to further separate train and validation sets, and combining different graphs to obtain stratified test sets for task-specific assessment.

The first configuration, which distinguishes similar pockets even for cases where ligands bind to alternative sites, was applied to a non-redundant single-ligand subset (PLINDER-NR, described in Section 3.2) to create the PLINDER-PL50 split which was used for retraining Diffdock. To better demonstrate the advantage of this split method, we evaluate our split against two more splits on PLINDER-NR also used to retrain DiffDock, four previously detailed splits mapped to PLINDER as described in Appendix A.4, and one additional high quality test set:

1. **PLINDER-Time**: Using January 1, 2021, as the cut-off date for the training set, all PLINDER-NR systems submitted after this date up to 2022-04-19 form the validation set, and those submitted afterward up to 2022-04-19 form the test set.

2. **PLINDER-ECOD**: This split was generated using the pocket-level ECOD topology (t-name) annotations. Systems from PLINDER-NR were first grouped by ECOD t-name and sorted by its number of members, the biggest group was added to train until the training set had 80% of systems. The rest of the groups were divided evenly into validation and test sets, along with systems with unknown t-name.

3. **DockGen split**: Another ECOD t-name derived split on a different dataset provided by DockGen (Corso et al., 2024).

4. **PDBBind-Original split**: This split uses the "general", "refined" and "core" sets of PDBBind (Liu et al., 2015) as train, validation and test sets respectively.

5. **PDBBind-DiffDock split**: This split was generated by removing ligands and receptors similar to the training set from the time-split PDBBind test set, used in DiffDock (Corso et al., 2023).

6. **PDBBind-LP**: A cleaned and reorganzied PDBBind split of non-covalent binders controlling for leakage defined by high protein sequence and ligand similarity (Li et al., 2024).

7. **PoseBusters** has recently gained popularity as an additional benchmark set for evaluating docking methods, due to its focus on higher quality systems. To include evaluations against PoseBusters, we excluded all PoseBusters PDB IDs from PLINDER-ECOD and PLINDER-TIME splits.

In Table A11 we present the fraction of leaked systems (defined in Section 2.3) for each split for different metrics and thresholds. We note that RDKit failed to obtain ECFP4 for a number of SMILES, which might effect the reported ligand similarity fraction of leaked systems values. We report these numbers for the different PLINDER splits in Table A14.

E. Retraining DiffDock

We re-train DiffDock using the NVIDIA BioNeMo Framework (bio) (FW) with an identical model size of 20.2M parameters for original DiffDock comparison. A Fused Adam optimizer was used a with learning rate of 0.001, and decay rates (β_1 and β_2) 0.9 and 0.999. A new feature of DiffDock in the BioNeMo FW is an Adaptive Batch Sampler during training. Due to the variable size of protein-ligand complexes, the memory requirements when loading the heterograph can vary. This algorithm pre-computes the memory requirement of each complex, and shuffles the batches to

accommodate the memory overhead. Effective batch size is 12-13. All models were trained on eight 80GB A100 GPUs for 200-400 epochs, and fully converge in 24-30 hours. For a full list of model hyperparameters, see Table A13.

F. Performance vs Leakage analysis

Previous studies suggested that reported deep learning method performance in general ligand pose prediction is overestimated due to information leakage between the train and evaluation sets (Corso et al., 2024; Li et al., 2024). This information leakage is commonly detected by employing similarity metrics that are used to compare test systems to those encountered in training. We employed multiple metrics for this purpose (see Appendix B) to estimate the extent of leakage for PLINDER and other dataset splits.

To assess the generalization ability, several recent studies used high performing examples with quoted ligand or protein sequence dissimilarity above or below a certain cutoff. For example, Krishna et al. (2024) used below 30% protein sequence identity and below 0.5 ligand Tanimoto similarity, to consider dissimilar protein and ligand, respectively. However, it remains unclear to what extent different similarity metrics inflate the performance.

As we chose to remove the high quality PoseBusters from PLINDER train / validation / test splitting, none of our PLINDER splitting approaches (time, ECOD, PL50) have dealt with active de-leaking for this subset. As a result, this provides a good representative sample for leakage-performance assessment using three different DiffDock models trained on three PLINDER splits. For each model we estimate the success rate comparing the most accurate (lowest RMSD to reference) prediction in Top 10 poses to 2 Å threshold. Figure A2 demonstrates the relationship across different metrics and thresholds relative to reported performance. In Figure A2A, we show the mean excess success rate observed for "leaked" test systems relative to the baseline (all test systems) as a function of "leakage", determined by train-test distance cutoff. Likewise, in Figure A2B and Figure A2C, we show success rate enrichment for leaked systems compared to all test systems and change in best pose RMSD as a function of leakage cutoff for various similarity metrics. Finally, Figure A2D shows the cumulative leakage fraction as a result of distance to train set. This analysis reveals that DiffDock performance has varied sensitivity for different type of information leakage. The pocket and PLI similarity metrics show the most sensitive difference in performance. Systems that share higher than 50 PLI similarity seem to contribute the most significantly to overestimated performance, while ligand similarity is hardly affecting DiffDock success. It is somewhat intuitive that for a rigid docking task the pocket specific interactions form the most sensitive information that result in inflated performance if leaked. However,

for different model architectures and especially for different tasks - this assessment should be repeated independently. To enable such evaluation and provide model developers with a better understanding of the factors affecting their prediction methods, we provide scripts to generate such leakage vs. performance plots across different similarity metrics and performance measures.

Table A10. Split configurations used and resulting leakage metrics

PARAMETER	CONFIGURATIONS			
	1	2	3	4
G	[POCKET LDDT ≥ 50]	[POCKET SHARED ≥ 20]	[PROTEIN SEQSIM ≥ 30]	[PLI SHARED ≥ 20, POCKET SHARED ≥ 50, PROTEIN LDDT ≥ 70]
D	[2]	[2]	[2]	[2, 2, 1]
SPLIT	NUMBER OF SYSTEMS			
TRAIN	279297	248849	339791	255463
TEST	14491	16910	4932	15132
VAL	19452	10131	17666	13896
REMOVED	122384	159734	73235	151133
SPLIT-PAIR	FRACTION OF LEAKED SYSTEMS			
PLI SHARED $\geq$ 50				
TRAIN VS. TEST	0.03	0.00	0.00	0.00
VAL VS. TEST	0.00	0.00	0.00	0.00
TRAIN VS. VAL	0.06	0.02	0.02	0.03
TRAIN VS. POSEBUSTERS	0.52	0.39	0.77	0.46
POCKET LDDT $\geq$ 50				
TRAIN VS. TEST	0.00	0.58	0.00	0.14
VAL VS. TEST	0.00	0.15	0.00	0.03
TRAIN VS. VAL	0.89	0.77	0.89	0.81
TRAIN VS. POSEBUSTERS	0.56	0.73	0.83	0.60
POCKET SHARED $\geq$ 50				
TRAIN VS. TEST	0.07	0.00	0.00	0.00
VAL VS. TEST	0.00	0.00	0.00	0.00
TRAIN VS. VAL	0.00	0.00	0.00	0.00
TRAIN VS. POSEBUSTERS	0.57	0.42	0.81	0.51
PROTEIN LDDT GLOBAL $\geq$ 50				
TRAIN VS. TEST	0.03	0.59	0.00	0.14
VAL VS. TEST	0.00	0.17	0.00	0.04
TRAIN VS. VAL	0.89	0.80	0.90	0.82
TRAIN VS. POSEBUSTERS	0.56	0.75	0.81	0.60
PROTEIN SEQSIM $\geq$ 30				
TRAIN VS. TEST	0.34	0.70	0.00	0.40
VAL VS. TEST	0.15	0.29	0.00	0.18
TRAIN VS. VAL	0.93	0.84	0.96	0.85
TRAIN VS. POSEBUSTERS	0.71	0.83	0.84	0.73
LIGAND SIMILARITY $\geq$ 30				
TRAIN VS. TEST	0.66	0.70	0.68	0.69
VAL VS. TEST	0.62	0.65	0.64	0.63
TRAIN VS. VAL	0.72	0.72	0.80	0.79
TRAIN VS. POSEBUSTERS	0.58	0.57	0.58	0.57

Table A11. Fraction of leaked systems between different dataset-splits for selected similarity metrics and thresholds. For PLINDER-splits we only report on high quality test structures

METRIC	PDBBIND -ORIGINAL	PDBBIND -LP	PDBBIND -DIFFDOCK	DOCKGEN	PLINDER -ECOD	PLINDER -TIME	PLINDER -PL50
PLI SHARED $\geq$ 50							
TRAIN VS. POSEBUSTERS	0.51	0.48	0.52	0.60	0.64	0.72	0.40
TRAIN VS. TEST	0.88	0.71	0.27	0.05	0.30	0.80	0.04
TRAIN VS. VAL	0.73	0.64	0.78	0.13	0.05	0.78	0.10
VAL VS. TEST	0.89	0.69	0.08	0.01	0.05	0.59	0.00
POCKET LDDT $\geq$ 50							
TRAIN VS. POSEBUSTERS	0.66	0.67	0.69	0.74	0.74	0.88	0.47
TRAIN VS. TEST	0.97	0.84	0.53	0.09	0.49	0.96	0.00
TRAIN VS. VAL	0.84	0.84	0.89	0.20	0.30	0.95	0.77
VAL VS. TEST	0.97	0.83	0.23	0.03	0.18	0.79	0.00
POCKET SHARED $\geq$ 50							
TRAIN VS. POSEBUSTERS	0.63	0.64	0.65	0.70	0.70	0.83	0.47
TRAIN VS. TEST	0.96	0.81	0.47	0.06	0.35	0.88	0.09
TRAIN VS. VAL	0.82	0.80	0.87	0.14	0.07	0.87	0.29
VAL VS. TEST	0.94	0.80	0.16	0.01	0.08	0.70	0.00
PROTEIN GLOBAL LDDT $\geq$ 50							
TRAIN VS. POSEBUSTERS	0.68	0.68	0.70	0.72	0.75	0.88	0.48
TRAIN VS. TEST	0.97	0.85	0.53	0.10	0.49	0.95	0.01
TRAIN VS. VAL	0.85	0.84	0.88	0.19	0.30	0.95	0.77
VAL VS. TEST	0.97	0.83	0.22	0.04	0.18	0.79	0.00
PROTEIN SEQSIM $\geq$ 30							
TRAIN VS. POSEBUSTERS	0.77	0.79	0.78	0.81	0.81	0.93	0.64
TRAIN VS. TEST	0.97	0.90	0.58	0.19	0.60	0.98	0.37
TRAIN VS. VAL	0.88	0.86	0.90	0.34	0.44	0.98	0.83
VAL VS. TEST	0.97	0.87	0.39	0.08	0.35	0.87	0.14
LIGAND SIMILARITY $\geq$ 30							
TRAIN VS. POSEBUSTERS	0.57	0.57	0.59	0.61	0.65	0.66	0.64
TRAIN VS. TEST	0.55	0.40	0.37	0.53	0.52	0.54	0.58
TRAIN VS. VAL	0.50	0.44	0.50	0.71	0.45	0.41	0.48
VAL VS. TEST	0.52	0.36	0.25	0.54	0.50	0.46	0.51

		TEST		POSEBUSTERS	
QUALITY	DATASET-SPLIT	TOP-10	TOP-1	TOP-10	TOP-1
LOW	PLINDER-ECOD	19.31 ± 0.28	13.57 ± 0.09	-	-
	PLINDER-TIME	37.61 ± 0.10	25.35 ± 0.50	-	-
HIGH	PLINDER-ECOD	26.47 ± 0.39	19.02 ± 0.24	47.17 ± 0.94	38.41 ± 2.11
	PLINDER-PL50	25.67 ± 0.61	18.19 ± 0.29	35.46 ± 2.09	29.41 ± 1.46
	PLINDER-TIME	58.75 ± 0.58	45.26 ± 0.38	58.16 ± 0.89	47.78 ± 0.24
HIGH + LOW	PLINDER-ECOD	20.85 ± 0.21	14.74 ± 0.11	47.17 ± 0.94	38.41 ± 2.11
	PLINDER-PL50	25.67 ± 0.61	18.19 ± 0.29	35.46 ± 2.09	29.41 ± 1.46
	PLINDER-TIME	41.78 ± 0.16	29.27 ± 0.42	58.16 ± 0.89	47.78 ± 0.24
	PDBBIND-DIFFDOCK (20M)	47.9	35.0	-	38.0
	PDBBIND-DIFFDOCK (30M)	57.0	43.0	-	50.0

Table A12. DiffDock performance on varied quality quality test sets reported as percentage success rate of prediction within RMSD <2 Å from reference for Top-1 and Top-10 ranked poses. For each PLINDER split, the trained model is evaluated on its corresponding test set and the PoseBusters set. For on PDBBind-DiffDock split, we show baseline values for the original DiffDock (20M parameters), and DiffDock-L (30M parameters).

Figure A2. Characterizing DiffDock PoseBusters benchmark performance relationship with distance cutoffs for different metrics. For this analysis we used an average performance of three models trained on PLINDER splits. The success rate was estimated for any of the top 10 poses being below 2 Å threshold from a reference pose. The effect of "leakage" distance cutoff for various similarity metrics on: (A) the excess success rate observed for "leaked" systems relative to the baseline, (B) Success rate enrichment factor, (C) change in best pose RMSD as a function of "leakage" cutoff (D) cumulative leakage fraction. We note the abrupt jump after 80% distance is due to our choice not to store pairwise similarities below 20% for our PLINDER dataset.
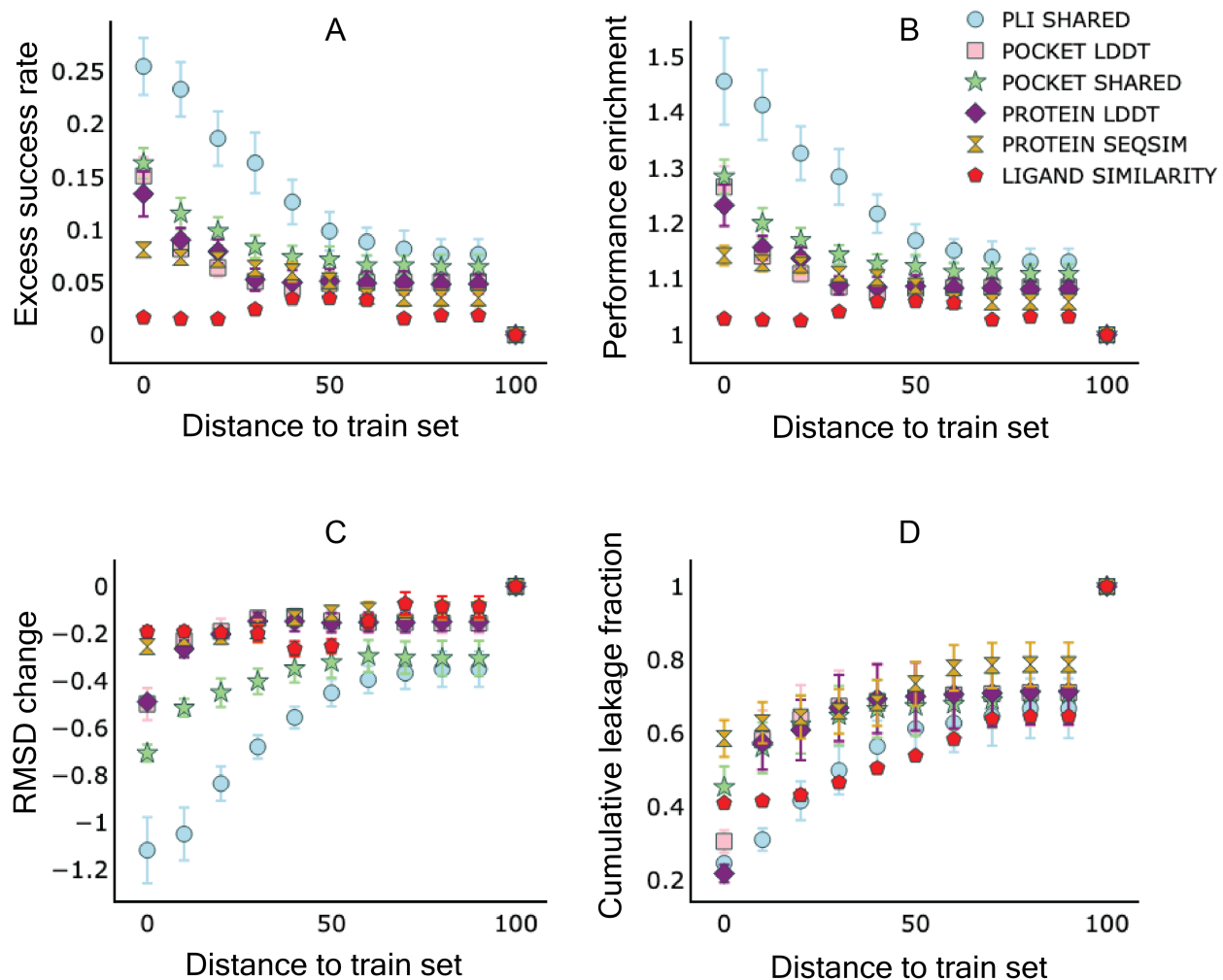
Table A13. Hyperparameters used for re-training the DiffDock Score Model. Choices are based on original publication model size and parameters, with the introduction of variable batch sizing.

Parameter	Option
Protein Graph	Coarse-Grain
ESM Language Model Embeddings	True
Ligand Hydrogens	False
Maximum Neighbors in Protein Graph	24
Receptor Radius	15
Distance Embedding Method	Sinusoidal
Dropout	0.1
Optimizer	Fused Adam
Learning Rate	0.001
Batch Size	Variable
Convolution Layers	6
Scalar Features	48
Vector Features	10
Total Parameters	20.2M

Table A14. Number of SMILES across the splits that failed to produce ECFP4 fingerprint with RDKit

CATEGORY	SPLIT	SIZE	NO. FAILED
PLINDER-ECOD	TEST	11401	186
PLINDER-ECOD	TRAIN	77411	757
PLINDER-ECOD	VAL	10169	158
PLINDER-TIME	TEST	10895	141
PLINDER-TIME	TRAIN	76950	804
PLINDER-TIME	VAL	11392	163
PLINDER-PL50	TEST	3517	12
PLINDER-PL50	TRAIN	57734	1888
PLINDER-PL50	VAL	3459	43